Chaos

Quantitative measure of memory loss in complex spatiotemporal systems

Cite as: Chaos **31**, 033126 (2021); https://doi.org/10.1063/5.0033419
Submitted: 15 October 2020 . Accepted: 23 February 2021 . Published Online: 08 March 2021

Miroslav Kramár, Lenka Kovalcinova, Konstantin Mischaikow, and Lou Kondic

View Online Export Citation CrossMark

AIP Publishing

© 2021 Author(s).

Quantitative measure of memory loss in complex spatiotemporal systems

Cite as: Chaos **31**, 033126 (2021); doi: 10.1063/5.0033419
Submitted: 15 October 2020 · Accepted: 23 February 2021 ·
Published Online: 8 March 2021

View Online Export Citation CrossMark

Miroslav Kramár,[1,a)] Lenka Kovalcinova,[2] Konstantin Mischaikow,[3] and Lou Kondic[2]

AFFILIATIONS

[1]Department of Mathematics, University of Oklahoma, Norman, Oklahoma 73019, USA
[2]Department of Mathematical Sciences, New Jersey Institute of Technology, University Heights, Newark, New Jersey 07102, USA
[3]Department of Mathematics and BioMaPS Institute, Hill Center-Busch Campus, Rutgers University, 110 Frelinghusen Rd., Piscataway, New Jersey 08854-8019, USA

[a)]**Author to whom correspondence should be addressed:** miro@ou.edu

ABSTRACT

History dependence of the evolution of complex systems plays an important role in forecasting. The precision of the predictions declines as the memory of the systems is lost. We propose a simple method for assessing the rate of memory loss that can be applied to experimental data observed in any metric space X. This rate indicates how fast the future states become independent of the initial condition. Under certain regularity conditions on the invariant measure of the dynamical system, we prove that our method provides an upper bound on the mixing rate of the system. This rate can be used to infer the longest time scale on which the predictions are still meaningful. We employ our method to analyze the memory loss of a slowly sheared granular system with a small inertial number I. We show that, even if I is kept fixed, the rate of memory loss depends erratically on the shear rate. Our study suggests the presence of bifurcations at which the rate of memory loss increases with the shear rate, while it decreases away from these points. We also find that the rate of memory loss is closely related to the frequency of the sudden transitions of the force network. Moreover, the rate of memory loss is also well correlated with the loss of correlation of shear stress measured at the system scale. Thus, we have established a direct link between the evolution of force networks and the macroscopic properties of the considered system.

Published under license by AIP Publishing. https://doi.org/10.1063/5.0033419

Understanding the global dynamics of nonlinear systems is typically challenging, especially if the governing equations are not known and only experimental data are available. A significant challenge arises from chaotic behavior, as this makes a precise long term prediction of future states impossible. While low dimensional chaotic dynamics is relatively well understood via the geometric theory of differential equations,[1,2] higher dimensional systems are usually treated using ergodic theory.[3,4] We propose a quantitative measure to assess the rate at which an ergodic system loses its memory, i.e., how fast the future states become independent of the initial condition. This method is computationally feasible and can be applied to experimental data observed in any metric space. The applicability of the method is demonstrated by considering a complex system of interacting particles modeling sheared granulars, where we show that the memory loss is related to the sudden transitions of the force network describing the interaction between the particles.

I. INTRODUCTION

The dynamics of chaotic systems is characterized by sensitive dependence on the initial conditions. This causes that the forecast accuracy decays with time. However, the rate at which the precision of predicted states declines is system dependent. There are different ways to quantify this rate, such as Lyapunov exponents,[5] entropy,[5] and mixing rate of the system. In this paper, we introduce a method for estimating the mixing rate.

We consider a dynamical system on a metric space X generated by a function $f\colon X \to X$ with an invariant measure μ. The invariant measure satisfies $\mu(f^{-1}(A)) = \mu(A)$ for all measurable sets and plays a central role in ergodic theory.[3] It provides information about the long term behavior of the system. For physical systems, there is usually a unique observable invariant measure that can be approximated from data.[5]

The invariant measure can be used to quantify the rate at which the trajectories starting from a set A mix in the phase space. Loosely

Published under license by AIP Publishing.

speaking, the set $f^n(A)$ is well mixed if $\mu(f^n(A) \cap B) \approx \mu(A)\mu(B)$ for all measurable sets $B \subset X$. If the set $f^n(A)$ is well mixed, then the fact that $x_0 \in A$ does not allow us to accurately predict $f^n(x_0)$. In particular, $f^n(x_0)$ can be in any set B with probability approximately given by $\mu(A)\mu(B)$. Hence, if the initial conditions inside the set A are indistinguishable due to a limited resolution, then our ability to predict the future declines with decreasing value of $|\mu(f^n(A) \cap B) - \mu(A)\mu(B)|$.

In this paper, we present a method for inferring the rate at which a discrete or continuous dynamical system loses its memory. For a continuous dynamical system, the map f^τ at the time scale τ is defined as follows. If $x(t, x_0)$ is the trajectory of the system with the initial point $x(0, x_0) = x_0$, then $f^\tau(x_0) = x(\tau, x_0)$. However, for computational purposes, it is preferable to choose a sufficiently small value of τ and consider the discrete dynamical system given by $f := f^\tau$. In order for the method to be applicable to experimental data, we do not require knowledge of f. We only need a finite sample $\{x_n\}_{n=0}^N$ of a trajectory starting from some initial condition x_0. The main idea is to analyze the cumulative distribution functions (CDFs), F_m^N, of the distances $\{d(x_n, x_{n+m})\}_{n=0}^{N-m}$ for different values of m. Theorem II.4 implies that, under certain conditions, the convergence rate of F_m^N can be used to estimate the mixing rate of the system.

The power of our measure is demonstrated by considering sheared granular systems consisting of a large number of interacting particles. One of the problems in analyzing such systems is that their description in terms of particles' positions and moments is incomplete since it does not capture the properties of the particle interactions. Even for the simplest case of a static system of (frictional) granular particles, the interaction field is not uniquely determined by the particle positions. Both physical experiments and simulations have shown that the forces acting between the particles form complex interaction force networks that are known to be crucial for understanding the mechanical properties of the system.[6] However, even these networks do not completely describe the state of the granular system and cannot be used to define its phase space.

In many applications, the dynamics cannot be observed directly in the phase space. Thus, it is essential that our method provides a meaningful estimate of the rate of memory loss if f is defined on an observation space that differs from the phase space of the system. Actually, we will show that for systems exhibiting symmetries such as granular systems,[7–9] it is more appropriate to infer this rate in a properly chosen observation space. This is due to the fact that the trajectories can move along the direction of a continuous symmetry, and the system can be losing its memory even if it is not mixing in the phase space.

To quantify the rate of memory loss in sheared systems, we analyze the time evolution of the interaction force networks. As already mentioned, there are many symmetries that can lead to drastic underestimating of this rate if our method were to be applied directly. To avoid this problem, we use the tools of algebraic topology to capture important properties of these networks.[9] In particular, we use persistence diagrams[10,11] to quantify the changes in topology of an interaction force network as the force level changes from infinity to zero.[12,13] In this way, each interaction force network is mapped to a point in a non-linear metric space of persistence diagrams. This mapping can be seen as a data reduction that quotients out the undesired symmetries. Thus, the space of persistence diagrams is well suited for the study of the dynamics of interaction force networks.[14,15]

By using our method, we shed new light on the dynamics of a simple shear flow of granular particles in the regime where inertial effects are strong and particles are stiff. We show that dependence of the rate of memory loss on the parameters of the system is nonlinear and not at all obvious. The global dynamics of the system changes erratically with the control parameter, suggesting the presence of bifurcations, even if the inertial number[16] is kept fixed. We also find that the rate of memory loss is closely connected to the frequency of abrupt changes in the persistence diagrams of the interaction force networks, triggered by a sudden reorganization of the network. Moreover, we demonstrate that these changes are correlated to system-wide average measures such as the shear stress.

The paper is organized as follows. The method for inferring the rate at which a discrete dynamical system loses its memory is introduced in Sec. II. Section III demonstrates its application to the dynamical systems generated by the tent map, logistic map, and to continuous time dynamical systems given by ordinary differential equations. Section IV deals with inferring the rate of memory loss in an observation space instead of the phase space. It also suggests how to obtain the correct rate if the system contains symmetry-related trajectories. In Sec. V, we analyze the dynamics of a large number of interacting particles modeling granular systems. Finally, in Sec. VI, we briefly discuss the challenges that might arise if the method is applied to experimental data.

II. MEMORY LOSS

Now, we present our method for inferring the rate at which a dynamical system loses memory. Let (X, Ω, d) be a measurable space with sigma algebra Ω and the distance function d. To ensure the applicability of the method to experimental data, we do not require knowledge of the function $f\colon X \to X$ generating the system. The method is based on the analysis of a finite sample, $\{x_n\}_{n=0}^N$, of a trajectory starting from some initial condition, x_0. From this sample, we compute the CDFs, F_m^N, of the distances $\{d(x_n, x_{n+m})\}_{n=0}^{N-m}$ for different values of m. We show that the convergence rate of the functions F_m^N can be used to assess the rate at which the memory is lost.

Naturally, a method is only useful if it does not depend on the choice of the initial condition, x_0. It turns out that a dynamical system generated by f can have more than one invariant measure. However, in many cases, the time evolution of physical systems produces well defined time averages.[5] This leads to a naturally selected measure, called the physical measure. For a dissipative system, this measure is concentrated on the attractor. Moreover, if $f\colon \mathbb{R}^k \to \mathbb{R}^k$ is a C^2 diffeomorphism with an Axiom A attractor A whose basin of attraction is U, then there is a unique invariant measure, μ, that produces well defined time averages.[17,18] To be more precise, there exists $V \subset U$, with the same Lebesgue measure as U, and for every $x \in V$, we obtain $\lim_{N\to\infty} \frac{1}{N} \sum_{n=0}^N \delta_{f^n(x)} = \mu$, where $\delta_{f^n(x)}$ is a Dirac measure concentrated on $f^n(x)$.

For systems with the abovementioned properties, $\lim_{N\to\infty} F_m^N = F_m$, where F_m is the CDF of the random variable $d(x, f^m(x))$ with x distributed according to μ. Thus, it is reasonable to expect that, for a large class of physical systems, the functions F_m^N do not

Published under license by AIP Publishing.

depend on the initial condition x_0 and approximate F_m well if the sample is long enough. Examples presented in Sec. III indicate how to detect that a sample is not sufficiently long.

In the rest of this section, we relate the convergence rate of the functions F_m to the rate of memory loss. For a set $A \in \Omega$, with $\mu(A) \neq 0$ and $m \in \mathbb{N}$, we define

$$\mathrm{mix}(A, m) := \mu^{-1}(A) \sup_{B \in \Omega} |\mu(A \cap f^{-m}(B)) - \mu(A)\mu(B)|,$$

which quantifies how well the trajectories starting from A are mixed at time m. The normalization factor, $\mu^{-1}(A)$, ensures that even a set A with a small measure has to be well mixed after m steps if the value of $\mathrm{mix}(A, m)$ is small. To assess the global rate of memory loss, we will consider partitions of the phase space X.

Definition II.1: *A collection of sets $\mathcal{T}$ is a partition of X if for all $A, B \in \mathcal{T}$*

1. $A \subset X$.
2. $A \cap B \neq \emptyset$ *implies that* $A = B$.

For a partition $\mathcal{T}$, we define its diameter

$$diam(\mathcal{T}) = \sup_{A \in \mathcal{T}} \sup_{x,y \in A} d(x, y)$$

and a measure of how well it is mixed,

$$mix(\mathcal{T}, m) = \sup_{A \in \mathcal{T}} mix(A, m).$$

To prove the convergence of the functions F_m, we have to require that the measure μ is bounded on neighborhoods of spheres, as is made precise in the following definition.

Definition II.2: *Let μ be a measure on the space (X, Ω, d). For $x \in X$, $s \in \mathbb{R}$, and $\varepsilon > 0$, we define*

$$S_{x,s}(\varepsilon) := \{\, y \in X \colon s - \varepsilon \leq d(x, y) < s + \varepsilon \,\}.$$

We say that the measure μ is S-bounded if there exists positive constants K and ϵ such that $\mu(S_{x,s}(\varepsilon)) \leq K\varepsilon$ for all $x \in X$, $s \in \mathbb{R}$, and $\varepsilon < \epsilon$.

The condition might look a bit strange, but as the following remark suggests, it is not overly restrictive.

Remark II.3: *If X is a compact subset of $\mathbb{R}^k$ and the measure μ on X has a bounded density with respect to the Lebesgue measure, then μ is S-bounded.*

Proof. Let g be the bounded density of μ with respect to the Lebesgue measure and $\epsilon > 0$. Choose R large enough so that the ball with radius R centered at the origin contains X. Then, $\mu(S_{x,s}(\varepsilon)) = \int_{S_{x,s}(\varepsilon)} g(x)dx$ is bounded by the volume of $S_{x,R}(\varepsilon)$ times $\max_{x \in X}(g(x))$. The volume of a ball with radius r in $\mathbb{R}^k$ is $\frac{\pi^{k/2} r^k}{\Gamma(k/2+1)}$; therefore, we can bound the volume of $S_{x,R}(\varepsilon)$ from above by $2\varepsilon k(R+\epsilon)^{k-1} \frac{\pi^{k/2}}{\Gamma(k/2+1)}$ for all $\varepsilon < \epsilon$. Thus, the measure μ is S-bounded. □

Finally, we are in the position to state the main theorem concerning the convergence rate for F_m. It shows that the convergence rate of F_m provides an upper bound on how fast the partitions with a decreasing diameter are mixed. We will demonstrate in Secs. III and V that this convergence rate is useful for inferring the rate of memory loss in the system.

Theorem II.4: *Suppose that $f \colon X \to X$ has an S-bounded invariant measure μ. Let $\{\varepsilon_m\}_{m=1}^{\infty}$ be a sequence of positive numbers converging to zero. If there exists a sequence of partitions $\{\mathcal{T}_m\}_{m=1}^{\infty}$ of X such that $diam(\mathcal{T}_m) < \varepsilon_m$ and $mix(\mathcal{T}_m, m) < \varepsilon_m$, then F_m converges to the cumulative distribution F of the distance $d(x, y)$ between two random variables x and y, which are i.i.d. according to μ.*

Moreover, there exists a constant $C > 0$ such that

$$||F_m - F||_{\infty} < C\varepsilon_m. \tag{1}$$

Proof. By definition,

$$F_m(s) = \mu(\{\, x \in X \colon d(x, f^m(x)) < s \,\})$$

and

$$F(s) = \bar{\mu}(\{\, (x, y) \in X \times X \colon d(x, y) < s \,\}),$$

where $\bar{\mu}$ is the product measure. It follows from the additive property of the measure that F_m and F can be calculated as

$$F_m(s) = \sum_{T \in \mathcal{T}_m} \mu(\{\, x \in T \colon d(x, f^m(x)) < s \,\}) \tag{2}$$

and

$$F(s) = \sum_{T \in \mathcal{T}_m} \bar{\mu}(\{\, (x, y) \in T \times X \colon d(x, y) < s \,\}). \tag{3}$$

For every set $T \in \mathcal{T}_m$, we choose a point $x_T \in T$ and define

$$B_{x_T,s} := \{\, x \in X \colon d(x_T, x) < s \,\}.$$

The following inequality follows from Eqs. (2) and (3) and the triangle inequality:

$$\begin{aligned} |F_m(s) - F(s)| \leq & \sum_{T \in \mathcal{T}_m} \big|\mu(\{\, x \in T \colon d(x, f^m(x)) < s \,\}) \\ & - \mu(\{\, x \in T \colon f^m(x) \in B_{x_T,s} \,\})\big| \\ & + \sum_{T \in \mathcal{T}_m} \big|\mu(\{\, x \in T \colon f^m(x) \in B_{x_T,s} \,\}) - \mu(B_{x_T,s})\mu(T)\big| \\ & + \sum_{T \in \mathcal{T}_m} \big|\mu(B_{x_T,s})\mu(T) - \bar{\mu}(\{\, (x, y) \in T \\ & \times X \colon d(x, y) < s \,\})\big|. \end{aligned} \tag{4}$$

To show that inequality (1) holds, we need to properly bound the individual terms of inequality (4).

We start by estimating the terms in the first sum. To do this, we denote the symmetric difference of two sets A and B by $A \Delta B$ and recall that $|\mu(A) - \mu(B)| \leq \mu(A \Delta B)$. The fact that $B_{x_T,s-\varepsilon_m} \subset B_{x,s} \subset B_{x_T,s+\varepsilon_m}$ for all $x \in T$ implies

$$\begin{aligned} &\{\, x \in T \colon d(x, f^n(x)) < s \,\} \Delta \{\, x \in T \colon f^n(x) \in B_{x_T,s} \,\} \subseteq \\ &\{\, x \in T \colon f^n(x) \in S_{x_T,s}(\varepsilon_m) \,\} = f^{-m}(S_{x_T,s}(\varepsilon_m)) \cap T. \end{aligned}$$

Now, by using $\mathrm{mix}(\mathcal{T}_m) < \varepsilon_m$, we obtain

$$|\mu(S_{x_T,s}(\varepsilon_m))\mu(T) - \mu(T \cap f^{-m}(S_{x_T,s}(\varepsilon_m)))| \leq \varepsilon_m \mu(T).$$

Finally, the measure μ is S-bounded; therefore,

$$\mu(T \cap f^{-m}(S_{x_T,s}(\varepsilon_m))) \leq \varepsilon_m K \mu(T) + \varepsilon_m \mu(T).$$

Therefore, the first sum in (4) is bounded by $\varepsilon_m(K + 1)$.

Published under license by AIP Publishing.

Now, we turn our attention to the second sum. Note that $\{ x \in T\colon d(x_T, f^n(x)) < s \} = f^{-m}(B_{x_T,s}) \cap T$. Using that $\mathrm{mix}(\mathcal{T}_m) < \varepsilon_m$, we can bound the second sum by ε_m. By a similar argument as in the case of the first sum, we can bound the last sum by $K\varepsilon_m$. We leave this to the reader. By combining the estimates for the individual sums, we get inequality (1) with $C = 2(K+1)$. □

III. APPLICATIONS

A. Tent map

We start by considering a classical example of a simple system producing ergodic dynamics, the tent map, on the unit interval $[0,1]$. The map is defined by $f(x) := 2\min\{x, 1-x\}$. The invariant measure of this system coincides with the Lebesgue measure on $[0,1]$, which is S-bounded. Therefore, we can use Theorem II.4 to estimate the convergence rate of $||F_m - F||_\infty$.

The local expansion rate of this system is equal to two. Moreover, for $n \in N$ and $i \in \{0, 1, \ldots 2^m - 1\}$, every interval $T_m^i = [i2^{-m}, (i+1)2^{-m}]$ is uniformly stretched to $[0,1]$ by f^m. This implies that for a fixed m and every measurable set $E \subset [0,1]$, the measure $\mu(f^{-m}(E) \cap T_m^i)$ is the same for all i. Because f preserves μ, it has to be equal to $\mu(E)2^{-m}$, which is exactly $\mu(E)\mu(T_m^i)$; therefore, $|\mu(f^{-m}(E) \cap T_m^i) - \mu(E)\mu(T_m^i)| = 0$. We consider the sequence of partitions $\{\mathcal{T}_m\}_{m=0}^\infty$, where $\mathcal{T}_m$ consist of the sets T_m^i for $i \in \{0, 1, \ldots 2^m - 1\}$. Note that $\mathrm{diam}(\mathcal{T}_m) = 2^{-m}$ and $\mathrm{mix}(\mathcal{T}_m) = 0$. Thus, Theorem II.4 implies that

$$||F_m - F||_\infty \le C2^{-m}. \tag{5}$$

The fact that the invariant measure, μ, coincides with the Lebesgue measure on $[0,1]$ makes it easy to calculate the limiting distribution,

$$F(s) = \begin{cases} 0 \text{ if } s < 0, \\ 2s - s^2 \text{ if } 0 \le s \le 1, \\ 1 \text{ if } s > 1. \end{cases}$$

The above formula allows us to study the convergence rate $||F_m^N - F||_\infty$ of the approximate distributions obtained from a finite sample $\{x_i\}_{i=0}^N$. We take $N = 5 \times 10^6$ and consider a trajectory starting from $x_0 = 0.1$. Due to the binary floating-point representation of the numbers in a computer, the direct iteration of the tent map does not produce a good sample of the trajectory. We use the fact that the tent map is homeomorphic to the logistic map with parameter $r = 4$ and define $x_n := \frac{2}{\pi}\sin^{-1}(y_n^{1/2})$, where y_n is a trajectory of the logistic map. From this sample, we calculate the CDFs, F_m^N, of the distances $\{d(x_n, x_{n+m})\}_{n=0}^{N-m}$ for different values of m.

Figure 1(a) suggests a convergence of F_m^N as $m \to \infty$. The value of $||F_m^N - F||_\infty$ is shown in Fig 1(b). The decay exhibited by $||F_m^N - F||_\infty$ is consistent with Eq. (5) only for $m \le 5$. For $m \ge 5$, the differences between the F_m^N and F are small, and to observe the predicted decay, one would need better approximations of F_m. A better approximation of the "spatial averages" F_m by the "time averages" F_m^N could be achieved by using a longer sample of the trajectory.

It might seem that the decay given by Eq. (5) is closely connected to the Lyapunov exponent, which is equal to $\ln 2$. However, Theorem II.4 shows that the convergence rate reflects the mixing rate, which has a more global nature than the Lyapunov exponent.

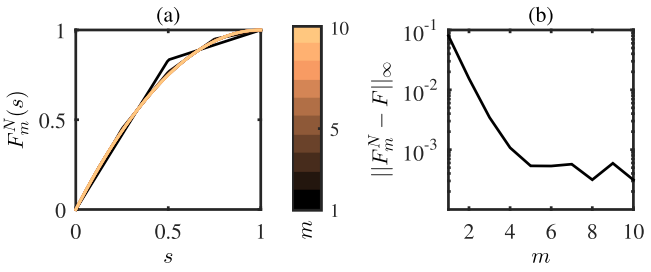

FIG. 1. (a) CDFs F_m^N of $\{d(x_n, x_{n+m})\}_{n=0}^{N-m}$ for the trajectory of the tent map starting at $x = 0.1$ and $N = 5 \times 10^6$. (b) Rapid decay of $||F_m^N - F||_\infty$ shows that F_m^N gets close to F as m increases.

To provide further intuition, we turn our attention to the study of the logistic map.

B. Logistic map

The logistic map on the interval $[0,1]$ is defined by

$$f_r(x) := rx(1-x),$$

where $r \in [0,4]$. For larger values of r, dependence of the dynamics on the parameter r is complicated and exhibits a large number of different bifurcations. This is documented by the erratic behavior of the Lyapunov exponents, shown in Fig. 2(a). We recall that the Lyapunov exponents measure the local expansion rate of the system and can be used to estimate the complexity of the dynamics.[5]

However, the rate of memory loss is a more global property of the system. For the dynamical systems defined on $\mathbb{R}^k$, it is often inferred from the decay of the autocorrelation function, $A_r(m)$,[19] depicted in Fig. 2(b). $A_r(m)$ switches between positive and negative values since a generic trajectory approaches different unstable periodic orbits that exhibit oscillations between large and small values during the consecutive iterations. For the values of r leading to the Lyapunov exponents $\lambda(r) > 0.3$, the decay rate tends to increase with r and is not directly correlated to the values of the Lyapunov exponents. For the value of r leading to $\lambda(r) = 0.054$, the visual inspection of the trajectory suggests a lack of mixing. Alternatively, the dynamics seems to be dominated by an unstable periodic orbit with period 8. This is in accord with the apparent periodicity of $A_r(m)$.

The advantage of our measure over the autocorrelation function is that it can be computed even if the phase space (observation space) of the dynamical system is non-linear because we only need to estimate the CDFs, F_m^N. In particular, to estimate the rate of memory loss for the system given by f_r, we generated a sample $\{x_i^r\}_{i=0}^{N=10^5}$ of its trajectory and computed the CDFs, $F_{m,r}^N$, of the distances $\{d(x_n^r, x_{n+m}^r)\}_0^{N-m}$ for different values of m. To prevent the clutter-ing of the notation, we omit r even though all functions in the rest of this section depend on r. In general, the limiting distribution F is not known, and one needs to estimate it. This can be done by using $F := F_m$ for m so large that the distributions F_m virtually do

Published under license by AIP Publishing.

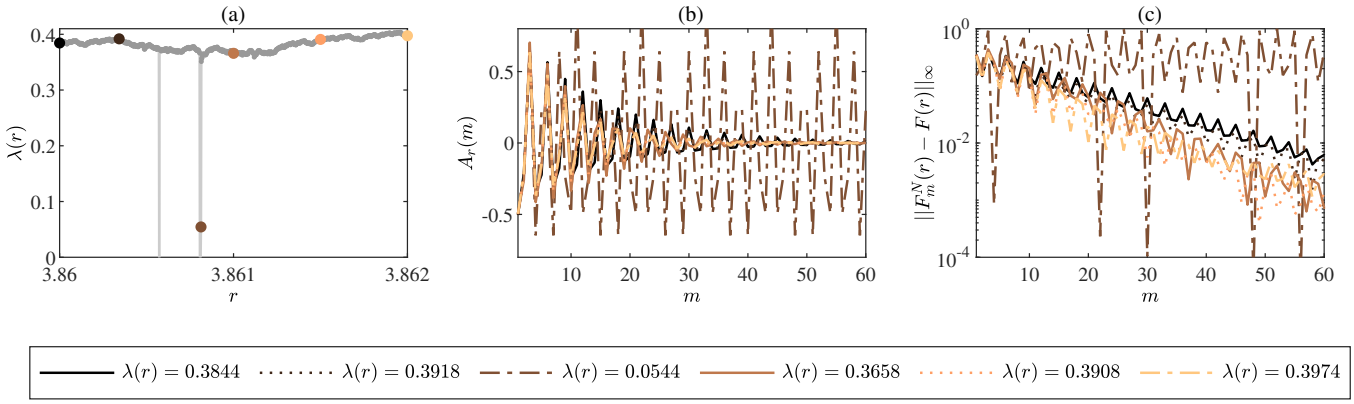

FIG. 2. (a) Lyapunov exponents $\lambda(r)$ for the logistic map for different values of the parameter r. Lyapunov exponents for the values of r considered in (b) and (c) are emphasized. (b) Autocorrelation A_r of the states for the logistic map for different values of r. (c) Decay of $||F_m^N - F||_\infty$ is faster for the systems exhibiting faster decay of correlations.

not change with m anymore. For the logistic map and the considered values of r, with $\lambda(r) > 0.3$, the distributions stabilize before $m = 100$. Thus, we use $F := F_{100}$.

Figure 2(c) depicts $||F_m^N - F||_\infty$. Clearly, the functions F_n^N do not seem to converge for the value r with Lyapunov exponent $\lambda(r) = 0.054$, indicating the lack of mixing. Similarly, to the correlation function, the decay rate of $||F_m^N - F||_\infty$ increases with r as long as $\lambda(r) > 0.3$. Hence, both measures indicate that the rate of memory loss for these systems increases with r. Moreover, note that the slope of the curves $||F_m^N - F||_\infty$ is well defined even at the places where the autocorrelation is already close to zero. This shows that there is a non-linear dependence between x and $f^m(x)$ even for $m \geq 30$, which cannot be captured by linear methods, such as autocorrelation function. Moreover, the slope of $||F_m^N - F||_\infty$ provides an upper bound on the rate of mixing.

C. Continuous dynamics

If the map f is a time τ map of a continuous dynamical system, then the behavior of the functions F_m provides information about important time scales of the system. Let us consider a differential equation $\dot{x} = h(x)$, where $x \in \mathbb{R}^k$, and suppose that f is its time τ map. Under the conditions mentioned earlier, the functions F_m can be estimated by a sufficiently long stroboscopic sample of a single orbit.

For a short time scale τ, the dynamics tends to be well approximated by the linearization of the system and $d(x(t), x(t+\tau)) \approx \tau ||h(x(t))||_2$, where $||\cdot||_2$ is the Euclidian norm in $\mathbb{R}^k$. By analyzing the scaling properties of F_m, one can detect the longest time scale at which the system is well approximated by its linearization. If the dynamics of $\dot{x} = h(x)$ is well approximated by its linearization at the time scale $m\tau$, then $d(x(t), x(t+m\tau)) \approx m d(x(t), x(t+\tau))$ and $F_m(s) \approx F_1(ms)$. This scaling is lost at the time scale at which the non-linear effects become important.

Similarly, as in Secs. III A and III B, the convergence of the functions F_m suggests that the system has a bounded attractor, and the rate of convergence of $||F_m^M - F||_\infty$ provides an upper bound on the rate of the memory loss.

IV. INFERENCE IN THE OBSERVATION SPACE

In Secs. II and III, we explained how to infer the rate at which a dynamical system loses its memory. The main idea was to measure the distances between the states along a sampled trajectory $\{x_n\}_{n=0}^N$. In particular, we concentrate on a discrete dynamical system given by $f\colon X \to X$, with an invariant measure μ defined on the measure metric space (X, Ω, d). However, in many applications, the dynamics cannot be observed directly in the phase space. Alternatively, one needs to rely on the measurements carried out in some observation space.

In the rest of this section, we suppose that there is a map $p\colon X \to Y$ from the phase space X to the observation space Y that relates the state of the system to the measured quantities. Under certain conditions, we can use similar ideas as before to infer the rate of memory loss. While the trajectory cannot be sampled in the phase space X, we can still obtain its sample $\{p(x_n)\}_{n=0}^N$ in the metric space (Y, d_Y). Similarly, as before, we define F_m^N as a CDF of $\{d_Y(p(x_n), p(x_{n+m}))\}_{n=0}^{N-m}$ and F as the CDF of the distance function $d_Y(p(x), p(y))$, where the random variables x and y are i.i.d. according to μ in X.

Using similar arguments as before, one can prove the exact analog of Theorem II.4 under the following assumptions. The map p is Lipschitz, and the pullback of the measure μ with respect to p is S-bounded; i.e., there exists a constant K such that for every $y \in Y$ and $s, \varepsilon > 0$,

$$\mu(p^{-1}(S_{y,s}(\varepsilon))) \leq K\varepsilon,$$

where $S_{y,s}(\varepsilon) := \{z \in Y\colon s - \varepsilon \leq d_Y(y,z) < s + \varepsilon\}$.

It turns out that for certain applications, it is preferable to infer memory loss in an appropriate observation space. The following example is motivated by physical problems that exhibit symmetries, such as Kolmogorov flow[20] and sheared granular systems.[7–9] Because

Published under license by AIP Publishing.

of the symmetries, a single trajectory can generate a set of symmetry-related trajectories that are dynamically equivalent. In particular, a trajectory can move along a direction of a continuous symmetry. To mimic this scenario, we consider a simple dynamical system on the cylinder $X = [0, 1] \times [0, 2\pi]$, where the end points of the second interval are identified to a single point. The dynamics is generated by the map

$$f(x, \theta) = (2 \min\{x, 1 - x\}, (\theta + \alpha) \mod 2\pi),$$

where $\alpha \in (0, \pi]$.

Indeed, the CDFs F_n^N of the sampled trajectory $\{(x_n, \theta_n)\}_{n=0}^N \subset X$ do not converge. Alternatively, for example, if α is rational, they change periodically with n. Therefore, our method identifies a lack of mixing. However, the precision of the predictions decreases with time in the same manner as for the tent map considered in Sec. III A. We can think of this scenario as a chaotic orbit drifting along the direction of a continuous symmetry θ. Thus, it is natural to quotient out this symmetry by using a projection $p(x, \theta) = x$. After applying this projection, our method correctly identifies that the rate of memory loss is the same as for the one dimensional tent map.

In general, eliminating the symmetries might not be so straightforward. For example, the symmetries in the sheared granular system depend on the properties of the particles and the precise geometry of the system. Defining a projection p that quotients out exactly the symmetries of this system is extremely complicated and computationally intractable. Although the map p defined by persistent homology is not completely understood, in our earlier work, we showed that persistent homology provides a useful tool for a quantitative description of the interaction force networks[12] that encode the mechanical properties of the granular material. Therefore, in Sec. V, we will study the evolution of interaction force networks in the space of persistence diagrams.

V. MEMORY LOSS OF SHEARED SYSTEMS

A. Simulations of linearly sheared systems: An overview

Now, we apply our method to simulations of sheared granular particles. The details of the simulation protocol are given in the Appendix. Here, we only provide a brief overview. To avoid as much as possible the complications involved in inhomogeneous flows, but also governed by the goal to consider experimentally realizable configurations, we consider the following setup. Two-dimensional frictional bidisperse circular particles (elastic disks) are placed between solid walls that impose shear flow (shear rate $\dot{\gamma}$) by moving to the right (top) and to the left (bottom) with the same speed, v. In what follows, all the relevant quantities are non-dimensionalized. We use the average particle diameter, mass, and binary collision time, τ_c, as the length, mass, and time scale, respectively (see the Appendix). To ensure uniform flow, the particles are placed on a solid substrate that moves with a linear velocity profile, similarly as in recent experiments.[21] The walls are subject to the applied pressure, P, chosen in such a way that the interaction forces between the particles are orders of magnitude stronger than the particle/substrate forces. In the present work, we vary both the shear rate and the applied pressure, while keeping the inertial number $I = \dot{\gamma}\sqrt{m/P}$ constant.

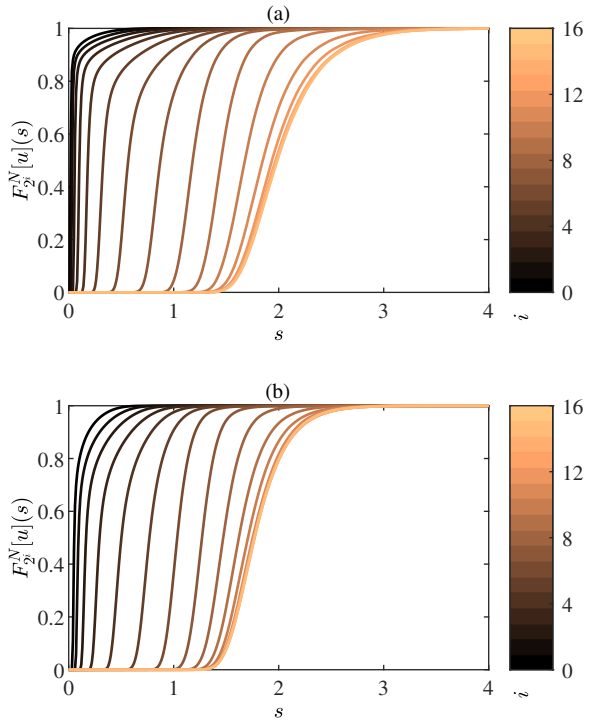

FIG. 3. $F_{2^i}^N[u]$ for the system (a) S_1 and (b) S_5. The value of i is indicated by the color bar.

There are three relevant time scales in the considered setup: $t_s = 1/\dot{\gamma}$ (shear time), $t_I = \sqrt{m/P}$ (inertial time), and $t_c = \sqrt{m/k_n}$ (binary collision time, also comparable to the time needed for a signal to propagate through a grain). One could also think of the typical contact time between the particles as a relevant time scale; however, for the simple shear flow considered here, this time is comparable to t_I. Out of these three time scales, one can produce two independent parameters; one possibility is to define $I = t_I/t_s$ and $\kappa = t_I/t_c$. Since $t_c \ll t_I \ll t_s$, $I \ll 1$ and $\kappa \gg 1$ (for the reference case, $I \approx 10^{-4}$ and $\kappa \approx 10^5$, see the Appendix). For such large values of κ, it has been argued that the main features of the flow are κ-independent and that the effect of a finite elastic modulus of the particles can be ignored.[16] Note that two simulations with different values of P and $\dot{\gamma}$, but with I and κ being the same, are identical after rescaling the time with t_s.

We take the simulations using $P = 1$ and $v = v_{ref} \approx 2.5 \times 10^{-5}$ as the reference case and refer to the system sheared with $v = uv_{ref}$ by S_u. For different values of u, we record the positions of the particles and the forces acting between them at the times $t_n = 2n\tau_c$, where $n = 0, \ldots, N = 5 \times 10^6$. By applying persistent homology to the interaction force networks recorded at the times t_n, we obtain a sequence $\{x_n\}_{n=0}^N$ that captures the evolution of the topological properties of the interaction force network along the sampled trajectory. To assess the differences between the persistence diagrams, we use the Wasserstein d_{W^2} distance, which mitigates the influence of noise.[12]

Published under license by AIP Publishing.

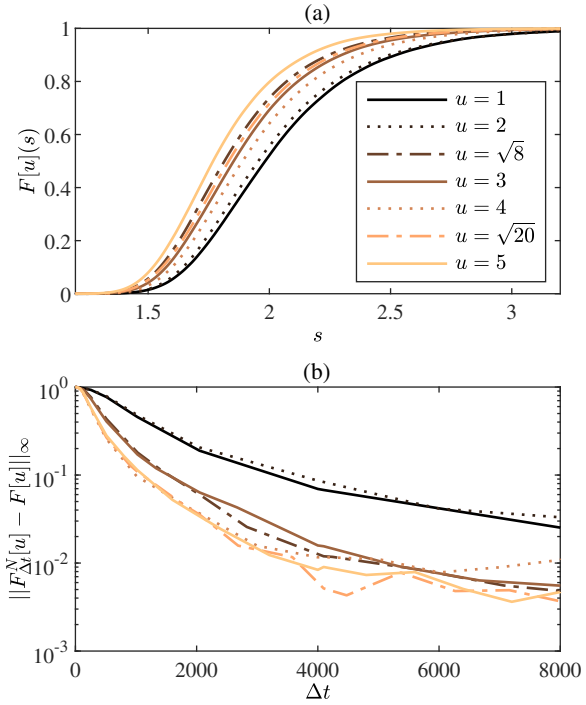

FIG. 4. (a) Estimated limiting distributions $F[u]$, given by $F^N_{215}[u]$, for different systems. (b) Value of $||F^N_{\Delta t}[u] - F[u]||_\infty$ as a function of Δt, where $\Delta t = 1$ corresponds to $2\tau_c$.

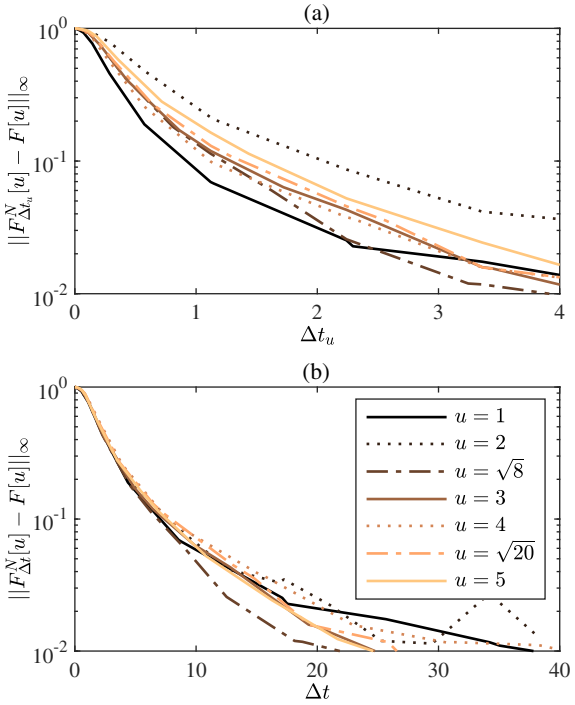

FIG. 5. (a) Value of $||F^N_{\Delta t_u} - F||_\infty$ as a function of Δt_u for different systems. Time t_u is scaled by the wall speed. (b) Value of $||F^N_{\Delta t^*_u} - F||_\infty$ as a function of Δt^*_u for different systems. Time t^*_u is scaled by the number of transitions.

B. Memory loss of linearly sheared systems

Now, we use our method to infer the rate of memory loss for the systems S_u. Using the sample $\{x^u_n\}_{n=0}^N$ of the system S_u, we compute the CDFs $F^N_m[u]$ of $\{d_{W^2}(x^u_n, x^u_{n+m})\}_{n=0}^{N-m}$. Figure 3 suggests that $F^N_m[1]$ and $F^N_m[5]$ converge. For every S_u, we have verified that the functions $F^N_m[u]$ do not depend on the initial conditions and change very little for $m \geq 10^4$. Hence, we approximate the limiting distributions $F[u]$ by $F^N_{215}[u]$. As documented by Fig. 4(a), the limiting distributions $F[u]$ vary with u, and there is no obvious trend. Thus, the asymptotic dynamics of the systems S_u changes in a rather complicated manner.

To study the systems S_u on the physical time scale, we denote a CDF of $\{d_{W^2}(x^u(t), x^u(t+\Delta t))\}$ by $F^N_{\Delta t}[u]$. Figure 4(b) shows $||F^N_{\Delta t}[u] - F[u]||_\infty$ as a function of Δt for different systems S_u. It indicates that the rate of memory loss increases with u but in a non-smooth fashion. This suggests a presence of bifurcations along the parameter u. The rate of memory loss increases with u as we pass over the consecutive bifurcation values, while it stays essentially constant away from these values.

Based on the earlier discussion about the expected minor influence of the elastic modulus, κ, it is natural to analyze memory loss by considering the time scaled by t_s. To be specific, we rescale the time by the wall speed in such a way that the wall moves by one particle diameter during one time unit. Using the rescaled time $t_u = t/(uv_{ref})$, we consider $||F^N_{\Delta t_u}[u] - F[u]||_\infty$ as functions of Δt_u. Figure 5(a) indicates that the decay rate of $||F^N_{\Delta t_u}[u] - F[u]||_\infty$ varies erratically with u.

This finding is surprising since, as mentioned earlier in the text, one would expect essentially identical behavior of the considered systems given that the inertial number I is kept fixed and the values of κ are large. To better understand this behavior, we recall that at the physical time scale, the rate of memory loss does not change much with u unless the parameter u passes through an expected bifurcation value. At those values, the rate increases with u; see Fig. 4(b). On the other hand, Fig. 5(a) shows that at the time scale t_u, the rate of memory loss decreases with u between the consecutive bifurcations, and this is consistent with the results obtained in Ref. 16.

Now, we connect the unexpected behavior shown in Fig. 5(a) directly to the evolution of the interaction force network. The animations (https://youtu.be/TutEfCInHJc and https://youtu.be/tY_sXanVP1M) indicate that this evolution exhibits slow–fast dynamics: the slow dynamics is dominated by a buildup of "force chains" that buckle, leading to large and fast rearrangements. We proceed to analyze these transitions and their possible connection to the memory loss.

To quantify the transitions, we consider the evolution of the systems at the fastest time scale given by our sampling. Let $D_u(t_u)$ be the d_{W^2} distance between the state of the system S_u sampled at time t_u and the next sampled state. The peaks of D_u, visible in Fig. 6, indicate

Published under license by AIP Publishing.

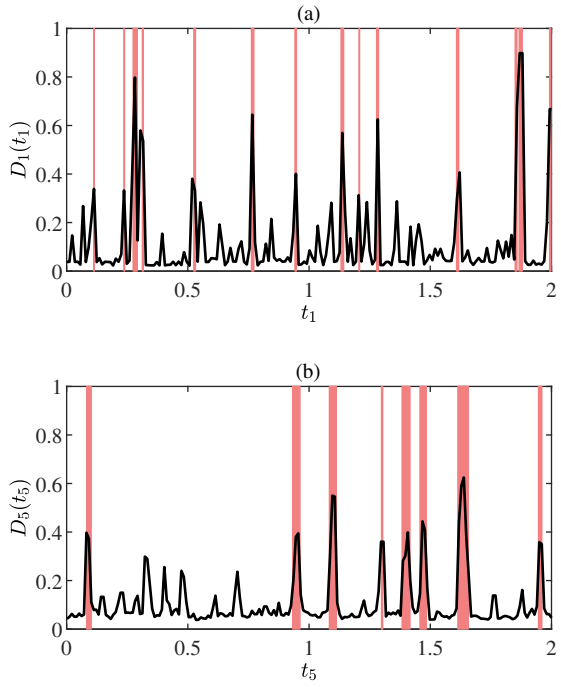

FIG. 6. Values of (a) $D_1(t_1)$ and (b) $D_5(t_5)$. The detected transitions are marked by red boxes.

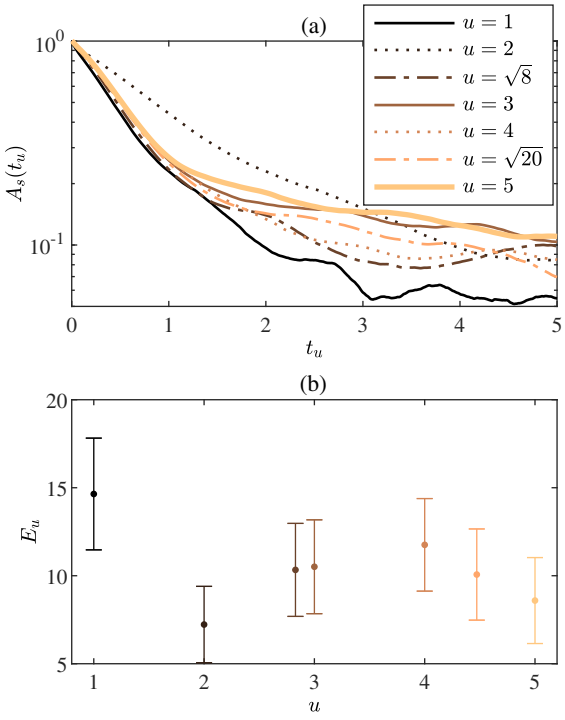

FIG. 7. (a) Autocorrelation of the shear stress as defined in the text. (b) Average number of transitions E_u of the system S_u during the time interval in which its wall moves by two particle diameters. The error bars indicate the standard deviation.

the presence of abrupt transitions of the system, which otherwise exhibits a relatively slow evolution. We define individual abrupt transitions as distinct peaks of D_u that exceed a threshold value of 0.3. While the exact number of detected transitions depends on the choice of the threshold, we find that the following results hold for thresholds in $[0.2, 0.4]$. Note that if $\bar{D}_u$ is the mean of D_u and σ_{D_u} is its standard deviation, then the interval $[\bar{D}_u + \sigma_{D_u}, \bar{D}_u + 3\sigma_{D_u}] \subset [0.2, 0.4]$ for each D_u.

Let δt_u be the average time between the two consecutive abrupt transitions of the system S_u and consider the rescaled time $t^* = t_u/\delta t_u$. Note that t^* does not depend explicitly on u but only on the number of transitions. Figure 5(b) shows that the values of $||F^N_{\Delta t^*}[u] - F[u]||_\infty$ are very similar for all systems S_u. This suggests that the rate of memory loss depends universally on the frequency of the transitions. Thus, we conjecture that the memory is predominantly lost during the abrupt transitions caused by localized buckling of the force chains.

Finally, we investigate the influence of the abrupt transitions on global measures such as the Cauchy tensor, defined by

$$\sigma_{ij} = \frac{1}{2A} \sum_{c_k,p} (\mathbf{F}_i r_j + \mathbf{F}_j r_i), \tag{6}$$

where A is the area of the domain, $r_{i,j}$ are the Cartesian components of the vector pointing from the center of particle p toward the particle contact c_k, and $\mathbf{F}_{i,j}$ are the corresponding interparticle force components. The sum is over all interparticle contacts c_k for all particles p, excluding the particle–wall contacts. Figure 7(a) shows the temporal autocorrelation of the shear stress (off diagonal component σ_{ij}). We see that the ordering of the autocorrelations for various values of u is similar to the ordering of the curves $||F^N_{\Delta t_u} - F||_\infty$; see Fig. 5(a). Moreover, only a handful of transitions occur before the autocorrelation drops below 0.2. Figure 7(b) shows the average number E_u of transitions of the system S_u during the time that the wall moves by two particle diameters. Figures 7(a) and 7(b) indicate that the systems with large E_u decorrelate faster, which further strengthens our hypothesis that the memory of the system is predominantly lost during the abrupt transitions.

VI. CONCLUSION

In this paper, we developed a method for estimating the rate of memory loss in complex spatiotemporal systems. We proved that our method provides an upper bound on the mixing rate of stationary systems satisfying some regularity conditions.

Many physical systems of practical interest involve nonstationary dynamics. There are at least two reasons for this. First, the physical system is stationary, but the dynamics has not yet settled on the attractor. Second, the system is non-autonomous, with time-varying parameters. In either of these cases, whether our methods apply or not depends on the considered time scale. If on the time scale at which our data are collected the trajectories continuously

Published under license by AIP Publishing.

drift across the phase space, then the distributions F_τ of the distances $d(x(t), x(t+\tau))$ between the states of the system (τ-time units apart) will not converge to a limiting distribution F. Thus, the lack of convergence identifies the lack of stationarity.

It is worth noting that in practice, the usefulness of our approach does not depend on stationarity. In the context of our simulation of the force networks of a granular system, we did not establish that the trajectory covers the full attractor (though we suspect that this is the case). Thus, it is possible that at a much longer time scale, the distribution F is different. Nevertheless, as shown in Fig. 3, we observe that the last half dozen curves indicate the time scale at which the distributions F_τ almost stop changing.

Therefore, if we consider a non-stationary system where the change in dynamics caused by the parameter shift is much slower than the evolution for the given parameter, then we would expect to see the same phenomenon: the evolution of the distributions F_τ will exhibit a similar pattern as in Fig. 3, a rapid change followed by a slow change due to the drift of the system. Nevertheless, the value of τ at which the rate of change of the distributions F_τ decreases considerably indicates the time scale on which the memory is lost.

In our study of time evolution of the interaction force networks in a sheared granular system, we have estimated the distributions F_τ by using 5×10^6 samples along a single orbit. Producing long samples of trajectories experimentally might be very challenging. Fortunately, this is not necessary since the distributions, F_τ, could be estimated from shorter samples of multiple trajectories by using a variety of well established statistical methods.[22] This estimate can be carried out even if some observations are missing or the sampling rate is not uniform. The only requirement on the data is that the individual trajectories are sampled at least for the amount of time exceeding the time scale on which the memory of the system is lost. It is important to mention that the quality of the estimated distributions F_τ will depend on the level and type of noise present in the data set. In particular, the estimated distributions will not converge. Alternatively, in the stationary case, they will fluctuate around the true limiting distribution. If the signal-to-noise ratio is not too small, then these fluctuations will be smaller than the initial changes of the distributions F_τ, and one can identify the value of τ at which they start to fluctuate around the limiting distribution.

The above challenges did not arise in our study of granular systems since we used simulated data. For these systems, we have shown that the dependence of the dynamics on the control parameters is very complex even for the simple case of uniform flow in a planar geometry. The rate of the memory loss depends erratically on the stiffness of the particles even if the particles are stiff and the inertial number is fixed. While proper understanding of this dependence should be the subject of future research, we have found that the rate of memory loss is strongly correlated with the frequency of abrupt transitions of the interaction force network. The fact that even a simple planar flow of circular particles exhibits an extremely complex dependence on the control parameters suggests that significant new research is still needed in the field of dynamics of dense granular matter. In particular, much more work will be needed to fully understand the systems exposed to more complex flows or the ones built from more complex particles.

ACKNOWLEDGMENTS

M.K. was supported by ERC Gudhi (No. ERC-2013-ADG-339025) and a Junior Faculty Fellowship from the University of Oklahoma. L. Kovalcinova and L. Kondic were partially supported by the National Science Foundation (NSF) (Grant No. DMS-1521717), the Defense Advanced Research Projects Agency (DARPA) (Contract No. HR0011-15-2-0033), and the Army Research Office (ARO) (Grant No. W911NF1810184). K.M. was supported by the NSF (Nos. DMS-1248071, DMS-1521771, DMS-1622401, and DMS-1839294) and the DARPA (Contract Nos. HR0011-16-2-0033 and FA8750-17-C-0054).

APPENDIX: PARTICLE INTERACTIONS AND A SIMULATION PROTOCOL

The particles in the considered system are modeled as 2D soft frictional inelastic disks that interact via normal and tangential forces, specified here in a nondimensional form. We use the average particle diameter, $\boldsymbol{d_{ave}}$, as the length scale, the binary particle collision time $\tau_c = 2\pi\sqrt{d_{ave}/(2gk_n)}$ as the time scale, and the average particle mass, m, as the mass scale. The force constant, k_n (in units of mg/d_{ave}), is set to a value corresponding to photoelastic disks.[23] The parameters entering the linear force model can be connected to physical properties (Young modulus, Poisson ratio) as described, e.g., in Ref. 24.

The dimensionless normal force between the ith and the jth particle is

$$\boldsymbol{F}^n_{i,j} = k_n x_{i,j}\boldsymbol{n} - \eta_n \overline{m}\boldsymbol{v}^n_{i,j},$$

where $\boldsymbol{v}^n_{i,j}$ is the relative normal velocity, $\overline{m}$ is the reduced mass, and $x_{i,j} = d_{ave} - r_{i,j}$ is the amount of compression, with $d_{ave} = (d_i + d_j)/2$ and d_i, d_j diameters of the particles i and j. The distance between the centers of the ith and jth particle is denoted as $r_{i,j}$. The parameter η_n is the damping coefficient in the normal direction, related to the coefficient of restitution set to $e = 0.5$.

We implement the Cundall–Strack model for static friction.[25] The tangential spring $\boldsymbol{\xi}$ is introduced between particles for each new contact that forms at time $T = T_0$ and is used to determine the tangential force during the contact of particles. Due to the relative motion of particles, the spring length ξ evolves as $\xi = \int_{T_0}^{T} \boldsymbol{v}^t_{i,j}(t)dt$, with $\boldsymbol{v}^t_{i,j} = \boldsymbol{v}_{i,j} - \boldsymbol{v}^n_{i,j}$ and $\boldsymbol{v}_{i,j}$ being the relative velocity of particles i, j. The tangential direction is defined as $\boldsymbol{t} = \boldsymbol{v}^t_{i,j}/|\boldsymbol{v}^t_{i,j}|$. The direction of $\boldsymbol{\xi}$ evolves over time, and we thus correct the tangential spring as $\boldsymbol{\xi} = \boldsymbol{\xi} - \boldsymbol{n}(\boldsymbol{n}.\boldsymbol{\xi})$. The tangential force is set to

$$\boldsymbol{F}^t = \min(\mu|\boldsymbol{F}^n|, |\boldsymbol{F}^{t*}|)\boldsymbol{F}^{t*}/|\boldsymbol{F}^{t*}|,$$

with

$$\boldsymbol{F}^{t*} = -k_t\boldsymbol{\xi} - \eta_t m\boldsymbol{v}^t_{i,j}.$$

Viscous damping in the tangential direction is included in the model via the damping coefficient $\eta_t = \eta_n$. The value of the normal spring constant is $k_n = 4 \times 10^3$, and parameters η_n and k_t are set to $\eta_n = 1.4$ (consistent with the specified value of $e = 0.5$) and $k_t = 0.8k_n$. The friction coefficient is set to $\mu = 0.7$.

In the simulations, the particles are placed on a base that moves with the speed that varies linearly from 0 to the speed of the top wall.

Published under license by AIP Publishing.

The purpose of the base is to ensure a linear velocity profile across the domain. There is a dissipative effect from friction between the particles and the base; for the ith particle,

$$-\mu_b |\boldsymbol{g}| \frac{\boldsymbol{a}_i(t)}{|\boldsymbol{a}_i(t)|},$$

where μ_b is the friction between the particle and the base and $\boldsymbol{a}_i$ is the acceleration of the ith particle. The magnitude and direction of $\boldsymbol{a}_i$ are determined here from the interaction of the particle i with all particles in contact,

$$\boldsymbol{a}_i = \frac{1}{m_i} \sum_{c_i} \boldsymbol{F}_{i,c_i},$$

where c_i runs over all particles in contact with particle i.

In our simulations, we integrate Newton's equations of motion for both the translational and rotational degrees of freedom using a 4th order predictor–corrector method with time step $\Delta t = 0.02$. Initially, particles are placed on a grid and given random initial velocity. Particles are bidisperse with the ratio of the large to small particle diameter 1.4. Approximately 1/3 of the particles have a large diameter and 2/3 of the particles have a small diameter. There are ≈1200 particles, and the rectangular domain is 54 particle diameters wide and 23 particle diameters high (in terms of d_{ave}).

Our simulations start by slowly compressing the domain with a specified pressure, $P = \mathrm{k}^2 P_0$, applied on the top wall until the top wall reaches a steady position. The system is then sheared with velocity $v = kv_0$, where $v_0 = 2.5 \cdot 10^{-5}$ (in the units of d_{ave}/τ_c). Walls are built of monodisperse particles with diameters of size d_{ave} placed initially at equal distances, d_{ave}, from each other. In the horizontal direction, the boundary conditions are periodic. The value of P_0 is found by compression of the top wall up to a packing fraction $\rho = 0.80$, ensuring a dense packing above the jamming point.

DATA AVAILABILITY

The data that support the findings of this study are available from the corresponding author upon reasonable request.

REFERENCES

[1] J. Guckenheimer and P. J. Holmes, *Nonlinear Oscillations, Dynamical Systems, and Bifurcations of Vector Fields* (Springer Science & Business Media, 2013), Vol. 42.
[2] C. Robinson, *Dynamical Systems: Stability, Symbolic Dynamics, and Chaos* (CRC Press, 1998).
[3] P. Walters, *An Introduction to Ergodic Theory* (Springer Science & Business Media, 2000), Vol. 79.
[4] K. E. Petersen, *Ergodic Theory* (Cambridge University Press, 1989), Vol. 2.
[5] J.-P. Eckmann and D. Ruelle, "Ergodic theory of chaos and strange attractors," Rev. Mod. Phys. **57**, 617 (1985).
[6] L. Papadopoulos, M. Porter, K. Daniels, and D. Bassett, "Network analysis of particles and grains," J. Complex Netw. **6**, 485 (2018).
[7] E. Aharonov and D. Sparks, "Shear profiles and localization in simulations of granular materials," Phys. Rev. E **65**, 051302 (2002).
[8] G. Lois, A. Lemaitre, and J. M. Carlson, "Spatial force correlations in granular shear flow. I. Numerical evidence," Phys. Rev. E **76**, 021302 (2007).
[9] J. A. Dijksman, L. Kovalcinova, J. Ren, R. P. Behringer, M. Kramár, K. Mischaikow, and L. Kondic, "Characterizing granular networks using topological metrics," Phys. Rev. E **97**, 042903 (2018).
[10] G. Carlsson, "Topology and data," Bull. Am. Math. Soc. **46**, 255–308 (2009).
[11] H. Edelsbrunner and J. L. Harer, *Computational Topology* (AMS, Providence, RI, 2010), pp. xii+241.
[12] M. Kramár, A. Goullet, L. Kondic, and K. Mischaikow, "Quantifying force networks in particulate systems," Physica D **283**, 37 (2014).
[13] M. Kramár, A. Goullet, L. Kondic, and K. Mischaikow, "Persistence of force networks in compressed granular media," Phys. Rev. E **87**, 042207 (2013).
[14] M. Kramár, A. Goullet, L. Kondic, and K. Mischaikow, "Evolution of force networks in dense particulate media," Phys. Rev. E **90**, 052203 (2014).
[15] L. Kondic, M. Kramar, L. Kovalcinova, and K. Mischaikow, "Evolution of force networks in dense granular matter close to jamming," EPJ Web Conf. **140**, 15014 (2017).
[16] F. da Cruz, S. Emam, M. Prochnow, J.-N. Roux, and F. Chevoir, "Rheophysics of dense granular materials: Discrete simulation of plane shear flows," Phys. Rev. E **72**, 341 (2005).
[17] R. Bowen and D. Ruelle, "The ergodic theory of Axiom A flows," in *The Theory of Chaotic Attractors* (Springer, 1975), pp. 55–76.
[18] D. Ruelle, "A measure associated with Axiom-A attractors," Am. J. Math. **98**, 619–654 (1976).
[19] S. Wiggins and J. M. Ottino, "Foundations of chaotic mixing," Philos. Trans. R. Soc. A **362**, 937–970 (2004).
[20] M. Kramár, R. Levanger, J. Tithof, B. Suri, M. Xu, M. Paul, M. F. Schatz, and K. Mischaikow, "Analysis of Kolmogorov flow and Rayleigh–Bénard convection using persistent homology," Physica D **334**, 82–98 (2016), Topology in Dynamics, Differential Equations, and Data.
[21] D. Bi, J. Zhang, B. Chakraborty, and R. P. Behringer, "Jamming by shear," Nature **480**, 355–358 (2011).
[22] L. Devroye and G. Lugosi, *Combinatorial Methods in Density Estimation* (Springer Science & Business Media, 2012).
[23] J. Geng, R. P. Behringer, G. Reydellet, and E. Clément, "Green's function measurements of force transmission in 2D granular materials," Physica D **182**, 274 (2003).
[24] L. Kondic, "Dynamics of spherical particles on a surface: Collision-induced sliding and other effects," Phys. Rev. E **60**, 751 (1999).
[25] P. A. Cundall and O. D. L. Strack, "A discrete numerical model for granular assemblies," Géotechnique **29**, 47–65 (1979).

Published under license by AIP Publishing.